energies

MDPI

Article

Power Quality State Estimation for Distribution Grids Based on Physics-Aware Neural Networks—Harmonic State Estimation

Patrick Mack *, Markus de Koster, Patrick Lehnen, Eberhard Waffenschmidt * and Ingo Stadler

Cologne Institute for Renewable Energies (CIRE) & Institute for Electrical Power Engineering, TH Köln, 50679 Cologne, Germany

* Correspondence: patrick.mack@th-koeln.de (P.M.); eberhard.waffenschmidt@th-koeln.de (E.W.)

Abstract: In the transition from traditional electrical energy generation with mainly linear sources to increasing inverter-based distributed generation, electrical power systems' power quality requires new monitoring methods. Integrating a high penetration of distributed generation, which is typically located in medium- or low-voltage grids, shifts the monitoring tasks from the transmission to distribution layers. Compared to high-voltage grids, distribution grids feature a higher level of complexity. Monitoring all relevant nodes is operationally infeasible and costly. State estimation methods provide knowledge about unmeasured locations by learning a physical system's non-linear relationships. This article examines a new flexible, close-to-real-time concept of harmonic state estimation using synchronized measurements processed in a neural network. A physics-aware approach enhances a data-driven model, taking into account the structure of the electrical network. An OpenDSS simulation generates data for model training and validation. Different load profiles for both training and testing were utilized to increase the variance in the data. The results of the presented concept demonstrate high accuracy compared to other methods for harmonic orders 1 to 20.

Keywords: harmonic state estimation; physics-aware neural networks; pruned artificial neural network; power quality state estimation

check for updates

Citation: Mack, P.; de Koster, M.; Lehnen, P.; Waffenschmidt, E.; Stadler, I. Power Quality State Estimation for Distribution Grids Based on Physics-Aware Neural Networks—Harmonic State Estimation. *Energies* **2024**, *17*, 5452. https://doi.org/10.3390/en17215452

Academic Editors: Dinko Vukadinović and Angela Russo

Received: 25 September 2024
Revised: 25 October 2024
Accepted: 28 October 2024
Published: 31 October 2024

Copyright: © 2024 by the authors. Licensee MDPI, Basel, Switzerland. This article is an open access article distributed under the terms and conditions of the Creative Commons Attribution (CC BY) license (https://creativecommons.org/licenses/by/4.0/).

1. Introduction

Conventional monitoring strategies in electrical power systems rely on the measured root mean square (RMS) voltages, currents, and power (active, reactive, and apparent). Phasor measurement units (PMUs) provide additional information about the relative voltage phasor's magnitude and angle. For power flow (PF) analysis, a measurement resolution of 15-min steps is typical and sufficient in most use cases. When it comes to measurements of power quality (PQ), various time intervals need to be considered. By definition, PQ is assessed through any deviation in the voltage's waveform from an ideal sinusoidal shape at an expected RMS voltage with a stable fundamental frequency [1]. Typical PQ disturbances are voltage sags or swells, flickers, harmonics, or short-period transient deformations. Characteristics for PQ are already considered in a wide range of standards (e.g., European EN50160 or EN61000-2-2). These standards necessitate the analysis of various parameters over time intervals ranging from milliseconds to hours [2,3].

PQ meters provide all relevant RMS values, voltage- and current phasors, various harmonic levels, flicker-evaluation, and high-resolution oscilloscope records to capture transient disturbances. Time-synchronizing these measurements via the precision time protocol (PTP) or Global Positioning System (GPS) enables applications like wide area monitoring systems (WAMS) [4]. WAMSs can be used to acquire the necessary data for PQ state estimation (PQSE), which describes various state estimation (SE) techniques for different PQ issues [5].

Assuming that a high penetration of distributed generation and electric vehicle charging in low- (LV) or medium-voltage (MV) grids influences PQ significantly, research and

simulations have been conducted to quantify this impact. The authors in [6] prove a strong contribution of large photovoltaic (PV) systems to harmonic distortion in Columbian distribution grids. Other sources discuss how smaller systems affect PQ. Using a simulation model, ref. [7] shows that PV systems connected to LV grids may cause considerable transient effects, voltage sags, and harmonics. Reference [8] analyzes the influence of electric vehicle charging in LV grids on technical equipment such as transformers. The authors propose to limit the current total harmonic distortion (THD) to 25–30% to preserve a reasonable life expectancy, as harmonic currents cause premature aging of components. Yet, another work observes current THD of up to 99% for the powerful, commercially available electric vehicle supply equipment (EVSE) of older generations [9]. Considering these influences on grid operation, distribution grid operators have an incentive to assess the level of harmonics and to identify the origins of PQ disturbances in LV and MV grids. Especially for live monitoring systems or WAMSs, this paper presents a high-performance estimation method suitable for application in near-real-time environments. Typically, this term is defined based on the specific application and refers to the system's processing time from the initiation of an event to the completion of transmission and evaluation [10]. In harmonic analysis, the shortest evaluation interval commonly used determines the performance requirements for SE. For example, the IEEE519 standard requires evaluation of voltage harmonics with an average interval of 3 s [11].

Summing up the described challenges, the following ideas form the central motivation of this research:

- Fast algorithmic execution time to deliver results in near-real time.
- Harmonic state estimation (HSE) on the base of a very small number of installed PQ meters.
- Application at both LV and MV levels.
- Assessment of the influence of integrating grid topology in HSE.

The primary research contribution of this paper is the evaluation of an SE method for analyzing harmonic flows in complex LV/MV mixed grids with sparse metering coverage.

2. State of the Art

HSE generates knowledge about harmonic quantities at unmeasured locations based on a specific set of measurements. Several algorithms for HSE in LV and MV grids can be found in the current literature. The following section will provide an overview of known methods for SE and HSE in distribution grids, as well as the benchmarking advantages of data-driven algorithms in this field.

2.1. State Estimation for Distribution Grids

Most SE algorithms rely on iterative processes that can also be applied to HSE. However, they are computationally expensive and require a large number of meters to achieve adequate observability of the grid's states. We will examine these aspects in detail in the results section of this article.

Some of these conventional methods for HSE include the weighted least squares (WLS) approach [12], singular value decomposition (SVD), which is a derivate of WLS for sparse measurement infrastructure [13,14], or Kalman filters (KF), which iterate over a time series of states [15]. Combining different approaches, such as the mutated two-loop particle swarm optimization as described in [16], can improve the precision of the basic algorithm. However, when these algorithms are applied to HSE, a higher ratio of PQ meters is needed for good convergence.

To provide an insight into an iterative SE process, the original WLS formulation by Schweppe [17] is briefly illustrated. The general formulation is defined by Equation (1).

$$z = h(x) + e \tag{1}$$

Here, z is a vector of real measurements, x is a vector of states to be determined, and $h(x)$ is a vector of functions that approximate the relationship to z by exploiting the physical dependencies given by the system's bus and branch admittances. e describes the error of the measurement devices. For M measurement locations, the objective function is as follows:

$$J(x) = \sum_{i=1}^{M} \frac{(z_i - h_i(x))^2}{R_{ii}} \tag{2}$$

R is the covariance matrix that contains the variances of each measurement location. These variances are considered to follow a Gaussian normal distribution with zero mean and are used to weigh different measurement types (e.g., PMU voltages, currents, power injection).

$$R = Cov(e) = diag\{\sigma_{11}^2, \sigma_{22}^2, \ldots, \sigma_{MM}^2\} \tag{3}$$

2.2. Neural Networks for State Estimation

To highlight the aforementioned difficulty of conventional iterative methods in maintaining observability with a small number of measurement devices, an example from [18] of a PF-SE based on WLS is presented. In this example, a distribution system is stated as unobservable with 31 nodes and 21 m locations.

Completely different scenarios are possible when applying data-driven methods, as demonstrated in [19]. This work performs a PF-SE by using an artificial neural network (ANN) in a 32-node distribution grid, which is observed by only three PMU measurements. This underscores the potential benefits of adopting more advanced statistical techniques, such as ANNs, for PQSE.

Another machine learning-based approach for SE is discussed in [20]. Here, an ANN is presented to apply PF-SE on a UK 95-bus network. The maximum time for estimating a system state among 88 samples was 0.7 s, while a range of non-data-driven works reported execution times of nearly a minute or more for convergence [12,21–23]. This highlights ANN applications for near-real-time computation tasks, too.

Accurate results for an ANN and simulation-based HSE considering the first 13 harmonic orders are presented in [24]. The author's concept takes probabilistic distributions of load and PV systems into account while processing smart meter data and sparse PMU measurements. A different approach based on ANNs is presented in [25]. Here, a generative adversarial network (GAN) is implemented. This combination of two ANNs is utilized for HSE and yields accurate results compared to a KF implementation.

Ref. [26] used a method of pruning connections in a dense ANN (DNN) to integrate physical knowledge of the grid's topology into the data model. This ANN architecture is known as physics-aware ANN (PANN) and will be applied in this work to incorporate information about infrastructure like connection dependencies of cables and transformers. According to [26], this method is especially suited for applications with a low coverage of measurements. The authors of this study demonstrate robust and precise estimation of fundamental frequency voltage phasors for distribution grids. The authors in [27] published the basis for the work in [26] and showed very short execution times for predictions with their PANN. Merely, 1.259 ms were needed to estimate the PF for 37 nodes. Compared to DNNs, the PANN is resilient against overfitting and vanishing or exploding gradients. The SE accuracy in comparison to traditional iterative methods is better for almost every tested scenario. Especially when sparse meter coverage impedes convergence for conventional algorithms, the PANNs still provide very good SE results. Since the static structure of the distribution grid is integral to the ANN architecture, a trained model requires updating the structure and retraining if the evaluation object changes.

Considering these benefits observed for PF-SE, we go one step further and evaluate a physics-aware approach in the context of PQ. Here, we apply PANNs for PQSE with a limited number of PQ meters and in complex MV and LV grids while maintaining low computational complexity.

2.3. Related Subject Areas in Power Quality State Estimation

Since SE is an approach to reduce costly measurements for extensive infrastructure, especially in the field of PQSE, it is desirable to use a minimum number of applied PQ meters, as these devices are very expensive.

Ref. [28] implemented and tested several methods for assessing PQ disturbances. The authors introduce a classification of error types to reduce the PQ phenomena to a limited set of algorithms. The presented article also employs this classification. Depending on the error type, the applied method varies. According to [28], the classifications depicted in Figure 1 consider the relevant criteria to assess PQ states.

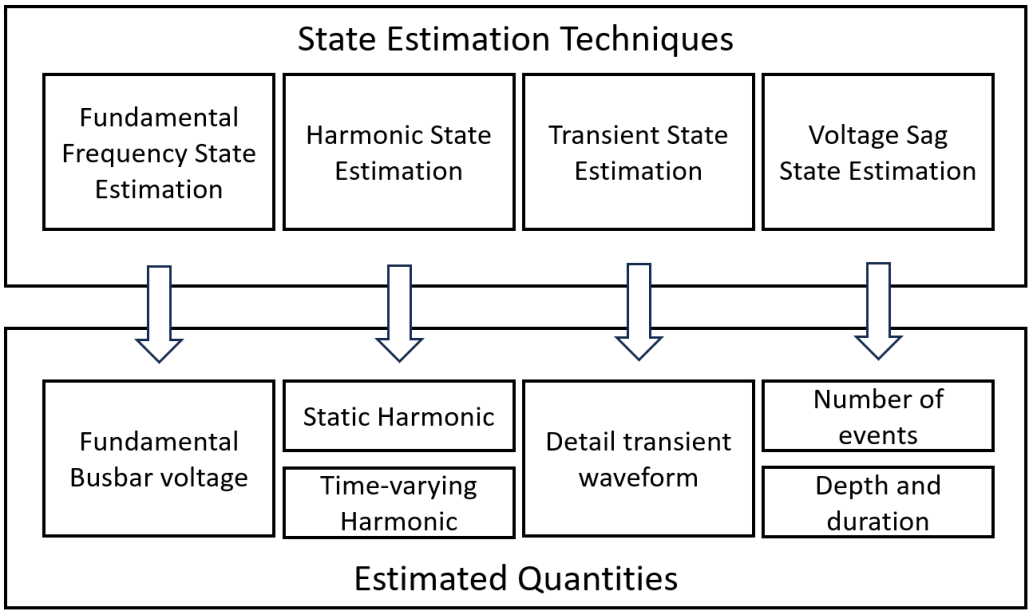

Figure 1. Classification of power quality state estimation techniques according to [28]. The four presented classifications cover the majority of PQ markers, or derivates of estimated quantities may be evaluated, e.g., a flicker can be calculated from fundamental frequency state estimation data.

Again, the applied methods are mainly WLS-based and may not be suitable for close-to-real-time applications. Fundamental frequency state estimation (FSE), voltage sag state estimation (VSSE), and HSE can be evaluated in the frequency domain. However, estimating transients in the time domain is a computationally costly process [28]. The numerical integrator substitution for transient state estimation (TSE) requires a lot of time, as every time step of interest needs to be calculated [29].

The presented work is embedded in a concept, which aims to combine TSE with FSE, and VSSE on the basis of the fast Fourier transform (FFT) and the presented HSE [30]. Works like [31,32] analyze and simulate transient data within the frequency domain. This method will be used in sparse mode (sFFT) to also apply the presented HSE model to different time domain signals as shown in [33].

3. Materials and Methods

Even though this work focuses on the evaluation of a fixed amount of harmonics in an HSE algorithm, it also provides a first insight into the utilization of the applied method for all previously mentioned fields of PQSE.

Therefore, this section contains the HSE formulation, information about the simulation, and specific details on the designed model. Finally, a general PQSE framework is put forward, within which the HSE is embedded.

3.1. Harmonic State Estimation Formulation

For HSE, the system state Equation (1) can also be applied by expanding the variables into matrices to account for all harmonics K. Specifically, z becomes an $M \times K$ measurement matrix, and x becomes an $N \times K$ state matrix, where M is the number of installed meters and N represents the number of estimated single-phase nodal voltage phasors (or states). Each complex nodal voltage $\underline{V}^k = V^k + jV^k$ (readings and states) considers K harmonic orders indexed by $k \in \{1, 2, 3, \ldots, K\}$. This yields the shapes of z and x as depicted in Equations (4) and (5).

$$z = \sum_{m=1}^{M} \sum_{k=1}^{K} \underline{V}_{mk} \tag{4}$$

$$x = \sum_{n=1}^{N} \sum_{k=1}^{K} \underline{\hat{V}}_{nk} \tag{5}$$

e describes the measurement error in the same dimensions as z. Rewriting (1) as follows illustrates the mismatch of the mathematical dimensions between $z - e$ and x.

$$h^{-1}(z - e) = x \tag{6}$$

Here, the inverse function h^{-1} is substituted by an ANN, which resolves this discrepancy.

This work aims to process snapshots of system states, as PMU-like PQ meters provide synchronized harmonic voltage phasors. These phasors are given in 3-s average intervals, or they can be obtained in custom dimensions from PQ meter fault recorders with typical sampling rates in the range of 10–40 kHz. Considering other applications in the context of PQSE, the model must not have any temporal dependencies, as it could be necessary to evaluate non-periodic waveforms. Therefore, time series may be evaluated step by step, but input data in consecutive steps are not needed for the algorithm.

3.2. Proposed Physics-Aware Neural Network

In general, ANNs are mathematical, data-driven models designed to mimic human learning processes. These models typically consist of at least three layers when calculating non-linear relationships. The basic architecture of ANNs usually includes an input layer, one or more hidden layers, and an output layer.

Each layer consists of an individual number of neurons that process numeric inputs from other neurons. Weight factors (w), adjusted during the training process, multiply the resulting interconnections. An activation function (σ), often a rectified linear unit (ReLU) or a hard tanh, processes the summed inputs of a neuron as its output (o) to the next layer [34–36].

Our proposed method (PM) tackles a supervised learning task, associating each feature set x with a corresponding output value y. The ANN aims at learning the mapping function from x to y. We want to evaluate the benefit of using the aforementioned PANN technology from [26,27] for HF. However, in comparison to [26], we aim to evaluate this concept for harmonic voltage phasors with a different sensitivity than the fundamental frequency. Also, this paper focuses on a fixed set of PQ meters and only on optimal placement for the shallowest possible depth of the PANN. We are not partitioning our grid, as we do not expect a lack of computational resources. Our here presented approach only uses a few PMU voltage measurements, where works such as [26,27] use PMU voltage, PMU current, and large numbers of pseudo measurements from historical data.

Figure 2a introduces a PANN implementation for the simple network depicted in Figure 2b. The PM uses this concept to integrate the network's structure, especially in HF for higher-order harmonics. Two case studies prove the strength of this method over conventional and other data-driven methods.

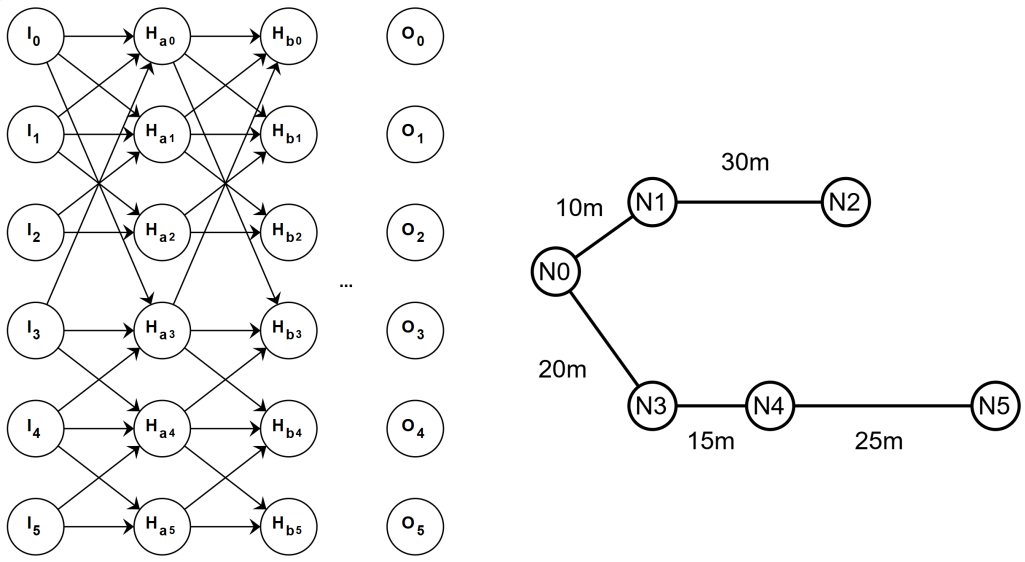

(**a**) (**b**)

Figure 2. In a PANN connections within the ANN correspond to physical connections from the electrical network. (**a**) Pruned ANN architecture. (**b**) Example of an electrical network with six nodes and five connecting lines.

3.3. Power Quality State Estimation Concept

Summing up the literature review and the physical framework of this work, a state estimation concept is proposed, considering four main components:

- Simulation environment for model training and validation
- Optional preprocessing for transients (time span isolation) with FFT analysis and synthesis (not part of this work)
- ANN estimator (few meters, close-to-real-time)
- Integration of the grid model (network connections)

According to the described components, the correlating block diagram is depicted in Figure 3. Training, validation, and testing of the model are solely conducted on simulation data.

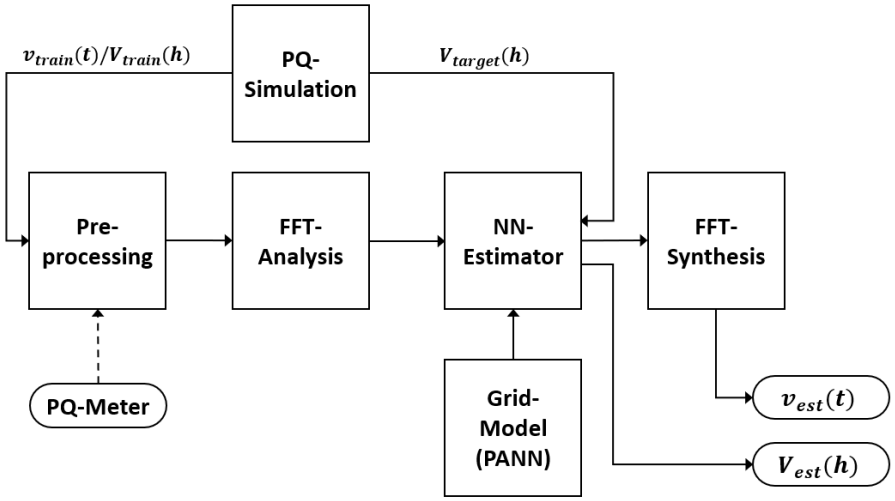

Figure 3. The suggested idea uses data from either simulation or PQ meters (dashed line). The simulation environment provides data in the frequency and time domain. Depending on the chosen input, FFT algorithms are employed. Outputs of the SE are either detailed voltage waveforms or complex nodal voltages of harmonics *h*.

This concept enables the evaluation of the fundamental frequency and harmonic components of the voltage signals as complex vectors. However, the Fourier transform yields complex coefficients for every frequency, which may not only include harmonics but also sub-harmonics, inter-harmonics, and supra-harmonics. The initial version of this estimator is only trained for a fixed range of 20 harmonics, omitting the FFT capabilities shown in Figure 3. Therefore, the training dataset does not currently include any other data.

3.4. Case Study Setup and Simulation

For concept evaluation, a simulation environment was set up to generate PF, HF, and electro-magnetic transient (EMT) data. Ref. [37] gives an extensive overview of EMT itself, waveforms, and simulation methods.

Figure 4 shows the simulated power grid, which was chosen to test the developed algorithms in depth due to its heterogeneous consumer structure (commercial, residential, industrial) and a typical rural distribution character of an LV/MV mixture [38]. The IEEE33-bus test system from [39] was also evaluated, but mainly for comparison with related work. Compared to the CIGRE LV grid, the second case study features only five non-linear loads, no generators, no transformers, and all nodes are at a medium voltage of 12.66 kV.

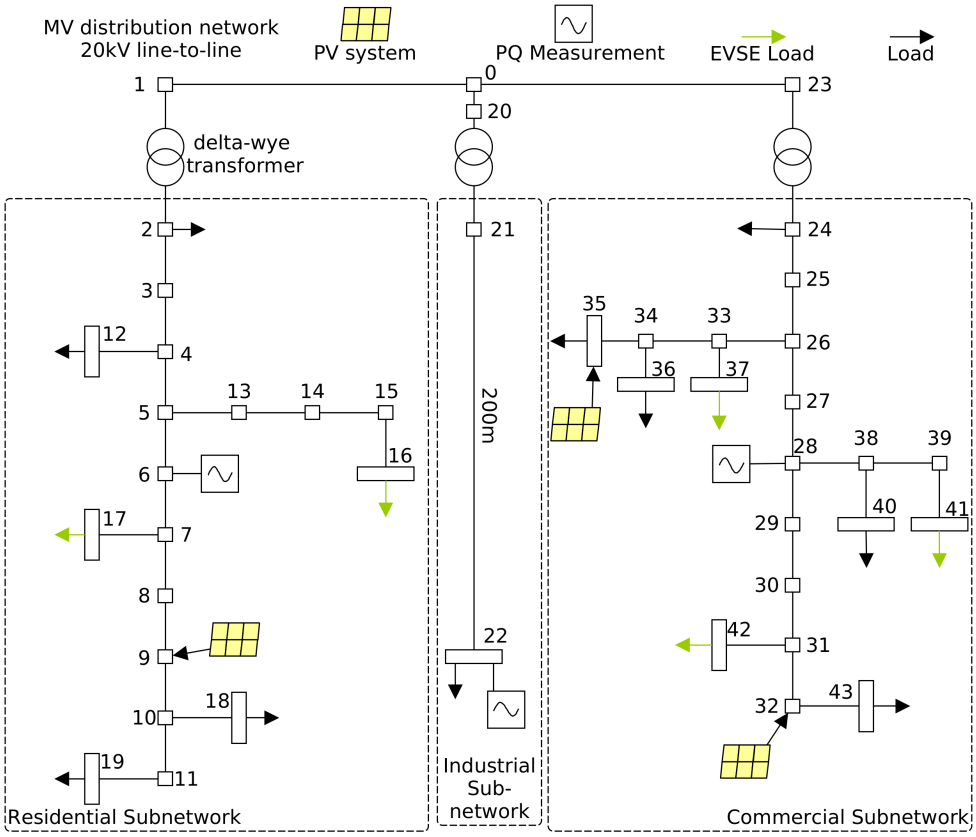

Figure 4. The heterogeneous distribution network for simulation and verification of harmonic state estimation concept [38]. We modified the original network to feature better harmonic characteristics. Three PQ meters are placed for estimation.

The OpenDSS simulation core was utilized to generate the training data for the reference grids. OpenDSS features various frequency-domain simulation modes like PF and HF [40]. A Python application drives the OpenDSS kernel via the OpenDSSdirect.py library. This application controls the time series profile input, simulation commands, and data output for every simulated node. The HF results were used to train a fully connected DNN, a convolutional ANN (CNN), and a PANN model. These models calculate theoretic values for the nodal voltages in the frequency domain.

Specific Extensions: The reference grid from [38] is extended by three PV generators (node 9: $P = 10$ kW, node 32: $P = 35$ kW, node 35: $P = 15$ kW), and five existing loads (nodes 16, 17, 37, 41, 42) are considered EVSE. Typical harmonic profiles realize harmonic current injection of these components. The other loads from [38] are considered linear and behave as constant power drains. All loads and generators are listed with their rated powers in Table A2 in the Appendix A.

Figure 5 depicts the lumped circuit equivalents that OpenDSS uses internally for lines and transformers. As the simulations may include frequencies relevant to resonances, the lines' capacitances need to be considered too. Therefore, Table 1 shows the full line parameters of the used types [41]. To also create reasonable propagation of harmonics along MV cables, the MV node was split up, and the slack at node 0 is connected to the three transformers through 100 m-long cables of type NA2XS2Y 1×95 mm² each.

Table 1. Line parameters used for the grid from [38] to model frequency dependencies accurately.

Line Types	R'_l [Ω/km]	X'_l [Ω/km]	C'_l [nF/km]
UG1	0.162	0.0832	210.0
UG2	0.2647	0.0823	210.0
UG3	0.822	0.0847	210.0
OH1	0.4917	0.2847	10.0
OH2	1.3207	0.321	10.0
OH3	2.0167	0.3343	10.0
NA2XS2Y 1×95 12/20 kV	0.313	0.132	216.0

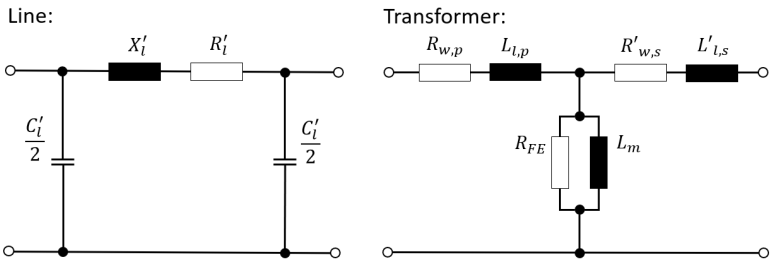

Figure 5. Circuit equivalents showing the considered components in the OpenDSS simulation. On the left, the typical π-equivalent for lines is depicted. On the right, a transformer with leakage inductances $L_{l,p}/L'_{l,s}$, winding resistors $R_{w,p}/R'_{w,s}$, main reactance L_m, and iron resistor R_{FE} is shown.

The transformers described in [38] lack shunt components. In OpenDSS, the shunt components are considered relative dimensions. R_{FE} is represented by the no-load losses p_{FE} and L_m corresponds to Equation (7).

$$i_{L,m} = \sqrt{{i_{mag}}^2 - {p_{FE}}^2} \tag{7}$$

Typical values for p_{FE} and i_{mag} can be found in [42]. In this work for smaller substations ($S_T < 1MVA$), $p_{FE} = 0.3\%$ and $i_{mag} = 3.0\%$ are used.

PV-, EVSE-, and Load Profiles and Spectra: In total, a time span of a complete year in steps of one minute was simulated to generate training data. Every single load, EVSE, and PV system received an individual load profile. The specific matching of load profiles, PV profiles, spectra and references can be found in [43]. In total, 525,600 simulated states are available for training, validation, and testing, but only 35,040 (15 min steps) were used for this article. Table A1 shows the spectra that were used to generate the test datasets.

3.5. Artificial Neural Network Architecture and Used Data

The used hyperparameters are depicted in Table 2. The Adam optimizer is used due to its suitability for large datasets and multidimensional regression learning [44]. Activation function leaky ReLU is used to reduce the risk of non-responsive neurons [34].

Training, Validation and Testing: The training set consisted of 70% of the used data, 20% and 10% for validation and testing, respectively. As mentioned beforehand, the test set was generated with unknown load profiles and partially different harmonic spectra to observe the networks' ability to generalize. These configurations can be found in [43].

Input and Preprocessing: In addition to the significance of training ANNs on normalized input, the complex voltages of PQ-meters may be split into Cartesian imaginary and real components. However, a special representation was tested and introduced to reduce the strong correlation between the imaginary and real components. Hence, the magnitude of the polar representation is used along with the imaginary part of $e^{i\phi}$ as input. Scaling is conducted by min/max normalization [34].

Table 2. Overview of the most important hyperparameters for implemented DNN, CNN and PANN.

Parameter	DNN	PANN	CNN
Batch-size	16,384	16,384	16,384
No. of hidden layers	2	6	7
Loss function	MSE	MSE	MSE
Activation	Leaky ReLU	Leaky ReLU	ReLU
Optimizer	Adam	Adam	Adam
Skip Connections	Yes	Yes	No

Multi-Layer Perceptron Architectures: In the hidden layers, three architectures were tested. The input layer was set to a dimension of $3 \times 2 \times 20$ (three complex voltage phasor measurements at 20 harmonics) for all configurations. The connections to the hidden layers were set up in different ways.

Initially, tests were conducted with two dense layers with a flattened shape of 1×1760 neurons (expecting 44 nodes with complex nodal voltages on the output layer at 20 harmonics). Architectures with more than two dense layers resulted in more trainable parameters. However, they yielded comparable or worse results. The second approach integrates the physical structure of the electrical grid into the connection scheme of the ANN, as explained above. Connections between the electrical network's nodes are considered by the adjacency matrix. The network's admittances are not considered.

For further comparison, a convolutional neural network (CNN) was implemented with similar hyperparameters. The convolutional layers start with a pointwise convolution (kernel: 1×1, stride: 1), then six depthwise convolutions (kernel: 3×3, stride: 1) are performed.

Figure 6 provides an overview of the PANN architecture compared to the simpler DNN and a CNN. The recursive Equations (8)–(10) describe the mathematical framework for the PANN without reshaping layers.

$$O_{i=0} = X + e_G \tag{8}$$

$$O_{i+1} = a_i(W_i^p \cdot O_i + B_i) \quad \text{with} \quad i = 0 \dots n \tag{9}$$

$$\hat{Y} = a_{n+1}(W_{n+1}^p \cdot O_{n+1} + B_{n+1}) \tag{10}$$

Index p marks the n pruned adjacency layers, while G notes a Gaussian layer, which is only active during training. It adds noise (e_G) to the input X. The weight matrices in the adjacency layers W_i^p prune connections by setting weights to zero. This iterative description represents the path from a complex input matrix X to the estimated matrix $\hat{Y}$.

Output-Data: All networks have output dimensions of $44 \times 2 \times 20$ (44 estimated complex nodal voltages at 20 harmonics). The activation function in the output layer is a linear function.

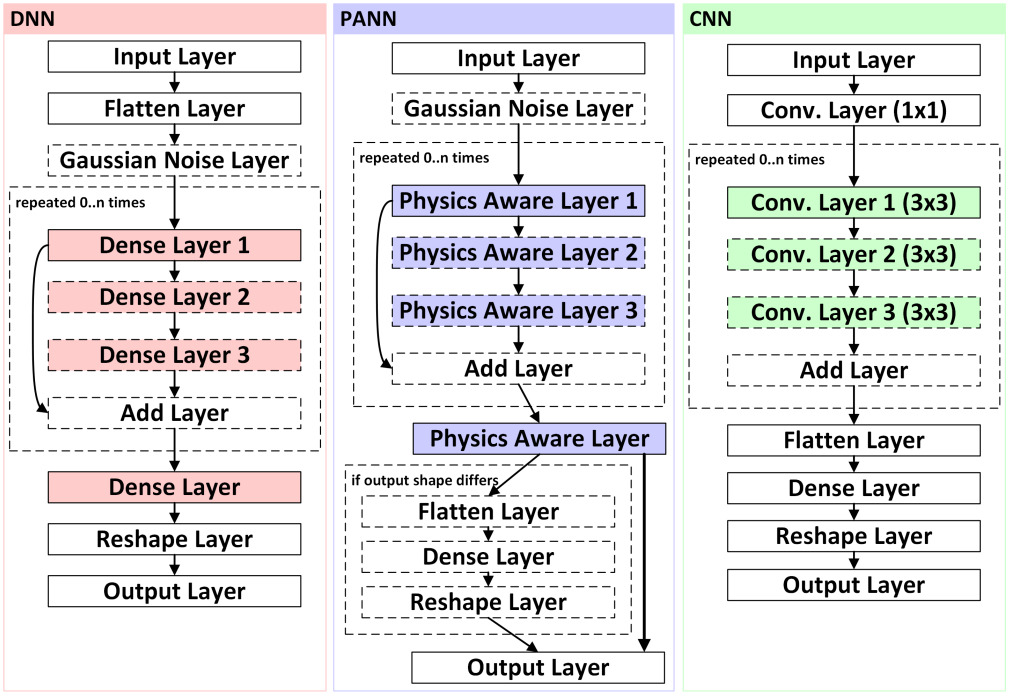

Figure 6. General overview of the compared architectures and layers used. The developed framework allows an individual number of layers. The DNN and the PANN models optionally use an additional noise layer on the input data. In this article, two dense layers, seven convolutional, and six physics-aware layers were used.

4. Results

The overall results show the best accuracy for the PANN solution. However, the complexity of setting up the model is significantly higher than using DNN or CNN topologies.

4.1. Error Metrics

The mean squared error (MSE) is used as the loss function during the training process and as an important benchmark. It is defined as follows:

$$MSE = \frac{1}{n}\sum_{i=1}^{n}\left(Y_i - \hat{Y}_i\right)^2 \tag{11}$$

The definition describes the average over n samples of the squared deviation of the estimate $\hat{Y}_i$ from a target value Y_i [45]. Another method that is used to provide insight into the presented model's precision is the mean absolute error (MAE). According to [46], the MAE is the most natural measure, and within this work, it gives a better physical interpretation. The MAE can be described as depicted below in (12).

$$MAE = \frac{1}{n}\sum_{i=1}^{n}\left|Y_i - \hat{Y}_i\right| \tag{12}$$

In [12] the normalized root MSE (NRMSE) was used for benchmarking and is defined as the root of the MSE over the datasets' mean $\overline{Y}$ [47].

$$NRMSE = \frac{\sqrt{\frac{1}{n}\sum_{i=1}^{n}\left(Y_i - \hat{Y}_i\right)^2}}{\overline{Y}} \tag{13}$$

The NRMSE will be used for comparison with related work from [12].

Additionally, the mean relative error (MRE) can be used to evaluate an estimator. Ref. [48] used the MRE as the metric for the presented HSE. Actually, the article mentions the MSE, but in correspondence with the authors [48], the following equation was provided:

$$MRE = \frac{1}{n}\sum_{i=1}^{n}\frac{|Y_i - \hat{Y}_i|}{|Y_i|} \tag{14}$$

4.2. Overall Results for CIGRE LV Case Study

Table 3 compares the final trained MSE loss of the tested networks. When the PANN is trained for more epochs, it significantly improves its accuracy, while the compared DNN only marginally improves. Generally, the compared CNN exhibits a higher validation loss within the conducted training. The MSE for 1400 and 3000 epochs is still higher than for the loss of the compared architectures.

Table 3. Overall network minimum MSE validation loss of all trained models over different amounts of epochs.

Epochs	DNN	CNN	PANN
1400	1.5×10^{-5}	3.6×10^{-5}	1.37×10^{-5}
3000	1.09×10^{-5}	1.16×10^{-5}	7.0×10^{-6}

Figure 7 emphasizes the accuracy of the PANN architecture over the entire validation dataset. A high curve's steepness correlates with little error over the majority of the test dataset. The PANN shows a better overall performance and only a few larger errors. Regarding the key challenge of presenting a precise HSE with sparse measurement equipment, the comparison of these ANN models is the most important demonstration of the effectiveness of the PANN-based HSE.

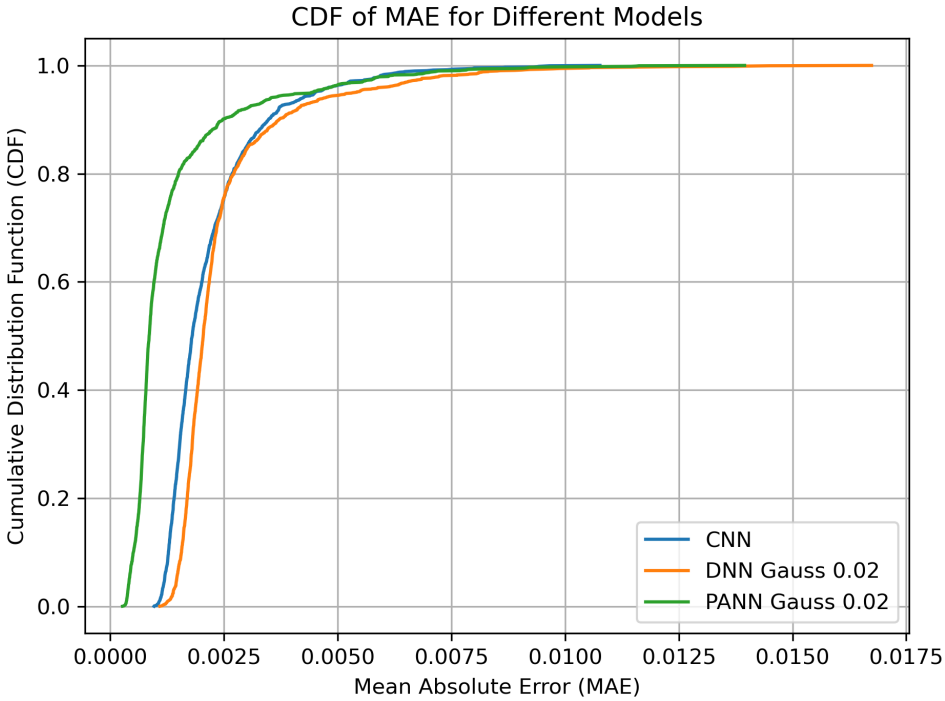

Figure 7. Comparison of cumulative distribution functions of the mean absolute errors within the test dataset for CNN, DNN and PANN architectures.

In order to observe the THD, Figure 8 gives an impression of the voltage THD (THD_V) for some nodes during a day in the test dataset. Typically, the THD is defined up to the 50th

order as shown in Equation (15) [11]. However, the highest order used may vary depending on the application and in this example, harmonic orders from 2 to 20 were considered.

$$THD_V = \frac{\sqrt{\sum_{n=2}^{50} V_n^2}}{V_1} \times 100\% \tag{15}$$

One can see that while predictions for nodes 16 and 25 show a good approximation, node 37 features an underestimation for higher THD levels. However, the trend of the curve is still followed by the estimator.

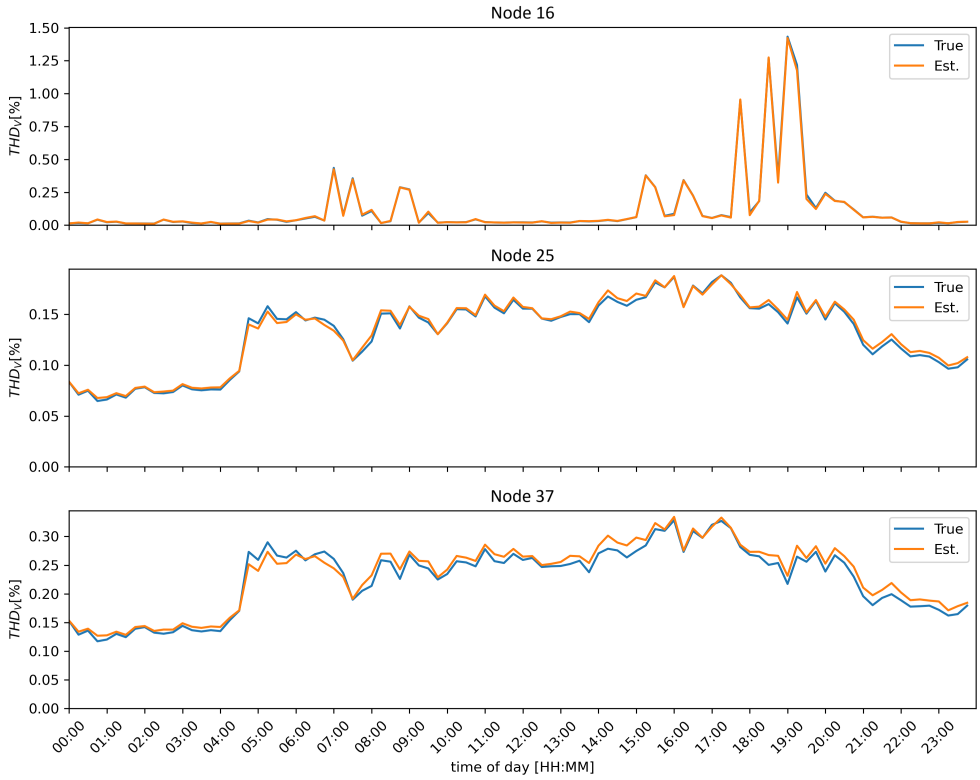

Figure 8. Example THD_V prediction of the PANN model over 24 h for example nodes across the reference grid.

Figure 9 compares the simulated values and the compared models' estimates of one system state with regard to the seventh harmonic order voltages. The precision of the PANN's guesses is remarkable compared to the DNN's and CNN's. Even when there is a slightly disturbed measurement on node 28, the network has a high ability to generalize. Additionally, for nearly every node, the DNN's performance is worse compared to the PANN's estimations.

Examining the individual harmonic magnitudes of the HSE, the heatmaps in Figure 10 illustrate the specific maximum MAE and maximum absolute errors individually for each node and harmonic frequency. For better comparability, all voltage magnitudes predicted for LV nodes are transformed to the MV level by the transformers' winding ratios ($\frac{n_{MV}}{n_{LV}} = \frac{20\text{ kV}}{0.4\text{ kV}} = 50$). Two different scales are used for the fundamental and harmonic frequencies to emphasize the differences, as harmonic voltages typically have significantly smaller magnitudes compared to the fundamental frequency.

In detail, one can see that nodes 33 to 37 and 41 to 42 have higher deviations among all odd harmonics. Notably, the 11th and 13th order harmonics appear difficult to predict in these regions of the grid. Focusing on the MAE evaluation, nodes 31 and 32 also show a considerable error of up to 0.6 V. However, the even harmonic orders (100 Hz, 200 Hz, 300 Hz, ...) on the mentioned nodes and the majority of both error metrics across all

nodes and frequencies exhibit very low error rates. Since the spectra used for EVSE do not show even harmonics, these HFs are not as complex compared to those of harmonic orders injected by PV generators and drawn by nonlinear loads, too.

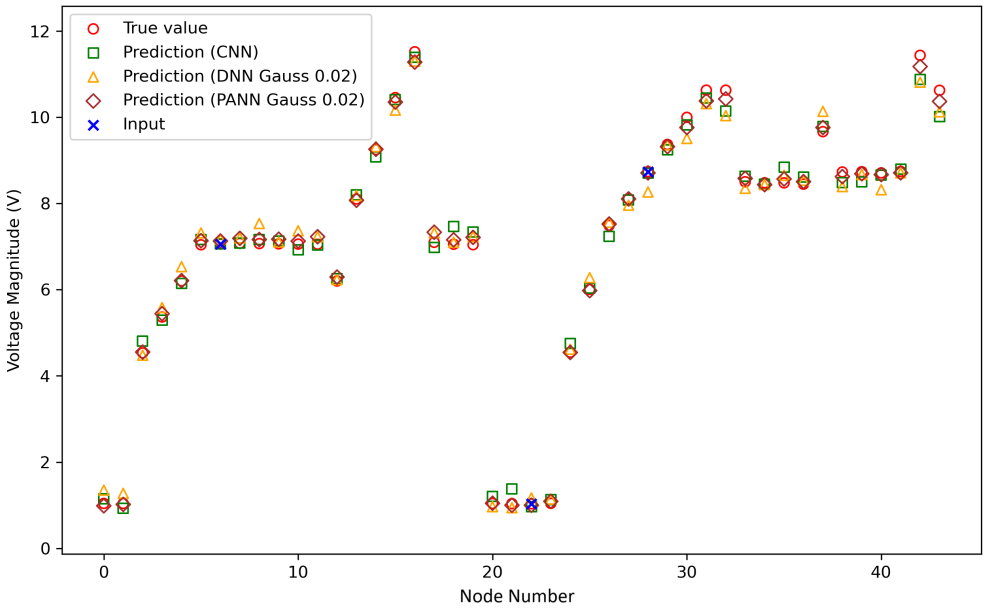

Figure 9. Example for an estimated state on seventh harmonic order. Voltages over all nodes are referenced to 20 kV level. Red circles represent the simulation data, blue crosses mark the placed meter position.

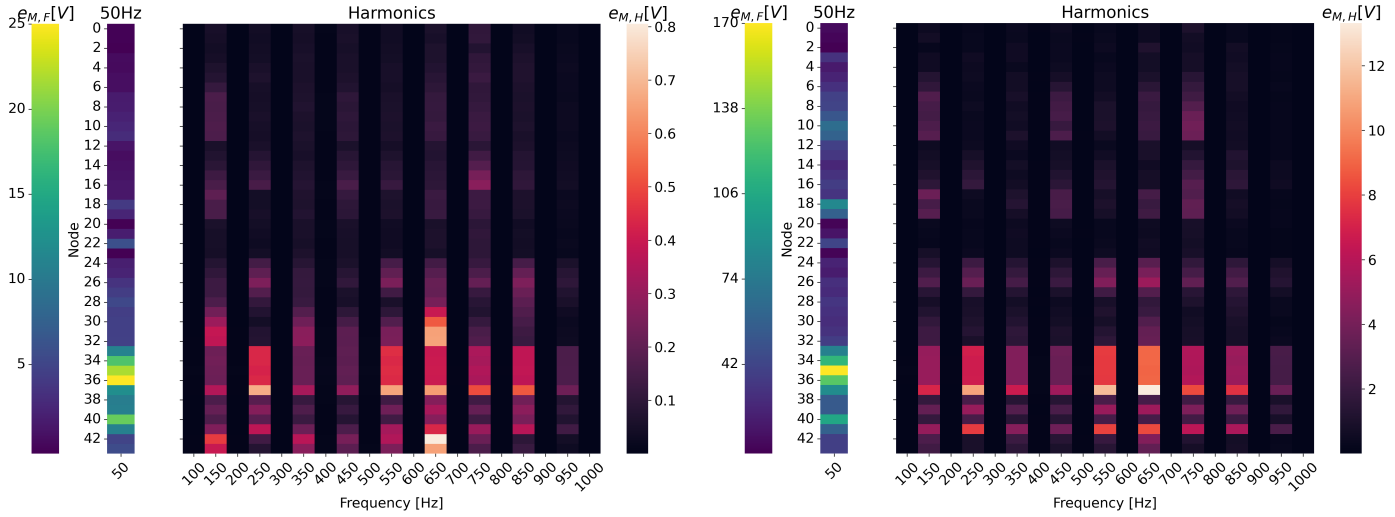

(**a**) (**b**)

Figure 10. Errors in magnitudes for the physics-aware model across the whole test set. (**a**) Mean absolute error of fundamental (F) and harmonics (H). (**b**) Maximum absolute error of fundamental (F) and harmonics (H).

Nodes 35 and 36 have a high maximum absolute error, as well as the highest MAE when it comes to estimating fundamental frequency values. This might be explained by the multiple branches within this section. Particularly around node 37, both an EVSE and a PV system are connected, leading to significant fundamental and harmonic currents along these lines. This substantially influences the harmonic levels as this subsystem exchanges high PF.

Overall, it is noteworthy that, across the entire test set, the maximum absolute error in fundamental voltages does not exceed 170 V (1.47% of the nominal 11,547 V line-to-earth voltage), with a maximum MAE of 0.22%.

4.3. Comparison with Related Work

Focusing on HSE, different algorithms can be found in the current literature. This section evaluates and compares the most significant works according to the following criteria:

- Estimated-Nodes-to-Meter-Ratio (ENMR)
- Individual Precision/Quality of Estimations
- Computational Performance/Execution Time

Estimated-Nodes-to-Meter-Ratio: To compare the amount of needed meter devices, the ENMR is introduced and defined as follows:

$$ENMR = \frac{n_e}{n_m} \tag{16}$$

n_e is the number of nodes in a network that are not measured and whose states will be estimated. The nodes, denoted by n_m, serve to collect measurement data.

Table 4 compares several works in the field of HSE for distribution grids. The ENMR shows that the PM is suitable for making good use of sparse measurement equipment. Only the study in [22] achieves a similar but still smaller ratio. It is also noteworthy that the presented concept monitors harmonics up to the 20th order, whereas works such as [12] consider the 15th order as the highest.

Table 4. Comparison of related work regarding grid complexity, ENMR, and estimated harmonic orders. Technique abbreviations: Modified Particle Swarm Optimization (MPSO), Sparse Bayesian Learning (SBL), Mixed-Integer Quadratic Programming (MIQP).

Ref.	Year	Method	Case Study Grid	ENMR	Harm. ord.
[13]	2016	SVD	IEEE13-bus	1.6	11
[22]	2011	MPSO	Radial 70-bus	10.67	13
[15]	2017	KF	IEEE13-bus	n.a.	n.a.
[24]	2020	SBL	IEEE13-bus	1.2	13
[14]	2017	SVD	Real 21-bus	2.0	13
[12]	2017	WLS	Indiv. 33-bus	3.13	15
[48]	2023	MIQP	IEEE33-bus	4.5	7
[49]	2023	Var.	IEEE33-bus	2.67	7
[25]	2023	GAN	IEEE33-bus	4.5	n.a.
PM	2024	PANN	CIGRE LV	13.67	20
PM	2024	PANN	IEEE33-bus	10.0	20

Individual Precision/Quality of Estimations: To achieve better comparability, the PM is also applied to the more common IEEE33-bus distribution system. The compared works [12,48] evaluate this feeder, too. The authors in [48] also compared their work to the SVD method from [13], these results are also listed. In order to emphasize the accuracy of certain harmonics, Table 5 compares these metrics individually.

Especially for the HSE proposed in [12], only four harmonic injections were considered, whereas our implementation of the feeder assumes five sources, like in [48]. Three PQ meters are placed on nodes 3, 13, and 29. Therefore, the ENMR is 10.

From the data given in [12], the NRMSE was evaluated for each node individually. The maximum value of the individual node NRMSE results is compared in Table 5. While the comparison of the NRMSE reveals better performance for estimation by the PANN at the fundamental frequency, the harmonic components are predicted similarly by the extended WLS method in [12].

Table 5. Comparison of related work and proposed method on the IEEE33-bus grid across all estimated nodal voltage phasors.

Metric	Maximum NRMSE		MRE		
Harm. ord.	PANN	WLS [12]	PANN	MIQP [48]	SVD [48]
1st	0.0023	0.0079	0.0009	25.226	2007.9
3rd	0.0847	0.0991	0.04628	0.0718	101
fifth	0.1948	0.0905	0.1163	0.0917	141
seventh	0.0592	0.0905	0.0388	0.1590	202

A different pattern occurs when comparing the MRE over the entire test dataset with the techniques in [48]. For harmonic orders 1, 3, and 7, the PANN provides better estimations than the compared methods. The MIQP and the WLS methods are able to predict the fifth harmonic more accurately. Notably, the PANN's fundamental frequency estimations exhibit very little MRE, while higher harmonics are in a similar range to the MIQP results. The significant difference in the first harmonic may be explained by the MRE definition, our large test dataset, and just a few larger absolute errors, as explained above in Figure 7.

Computational Performance/Execution Time: Especially when comparing the PM to conventional SE techniques like WLS, execution time is an important aspect for benchmarking. The presented study in [12] compared execution times for WLS (54.39 s) with other methods from [21–23] (all $>$ 1 min) for estimations up to the 15th order. In comparison, the PANN estimates the entire test dataset (3504 harmonic states) within an inference time of 1.44 s on an Intel® Core™ i7-12700K with a 25 MB cache and a CUDA NVIDIA RTX A2000 graphics processor.

4.4. Influence of Noisy Measurement

To transfer this concept to real-world applications, the influence of noisy measurements was also considered. The authors in [50] suggest error modeling by using Gaussian noise for PMU measurements. Authors of related work [51] propose noise modeling with zero mean and $\sigma = 0.01$ for voltage magnitude measurements in PF applications to increase the robustness of the model. To compensate for similar effects, the models presented in this work can be trained with an optional Gaussian noise layer. The influence is presented in Table 6. The validation loss MSE of different combinations is used as a marker over two test states. In the case of an ideal input value, the Gaussian layer will reduce the prediction's accuracy slightly by 19.6% and 12.7%. However, when a noisy input is applied to the network, the precision of the predicted states is improved by 6.3% and 9.7%. This positive effect occurs because the ANNs have already learned to generalize during training on slightly altered data. This test is an indication to use the Gaussian layer as a possible improvement for application in real grids, where noisy measurement data are expected.

Table 6. Minimum MSE loss on the validation set with and without input noise ($\sigma = 0.01$) and Gaussian layer with $\sigma = 0.02$ in two trial runs of PANN models trained over 3000 epochs.

	Ideal Input		Noisy Input	
Trial	-	Gauss. Lay.	-	Gauss. Lay.
1	5.45×10^{-6}	6.52×10^{-6}	8.58×10^{-6}	8.04×10^{-6}
2	5.75×10^{-6}	6.48×10^{-6}	8.93×10^{-6}	8.06×10^{-6}

5. Discussion and Conclusions

We implemented a highly accurate HSE that focuses on harmonic and fundamental flows within a typical distribution grid topology. In direct comparison with a DNN and a CNN architecture, integrating the grid's physical structure significantly reduces the validation loss by up to 35.78%. The network's short inference time of 1.44 s for estimating 3504 system states demonstrates the potential for near-real-time applications.

Measurement devices at three nodes, measuring only nodal voltages, are sufficient to estimate 41 complex state variables per 20 harmonic frequencies in a highly branched distribution grid. The presented case study exhibits three substations, two voltage levels, eight non-linear loads and generators, and five linear loads.

The latest literature does not present comparable precision at the given ratio of monitored locations to the number of states. Other articles, which have similar error rates on certain harmonics, use either more measuring devices or require at least about 1 min computational time for predictions. Although the second case study on the IEEE33-bus grid qualitatively demonstrates improved precision compared to other HSE methods, the focus should be on comparing ANN-based models, as in the CIGRE LV grid study. Given the challenge of performing HSE with sparse measurements, data-driven ANNs can predict nodal voltages, whereas conventional algorithms fail to converge. This work is among the first to apply HSE in LV grids, with the CIGRE LV case study as the primary focus. The results also confirm the effectiveness of the PANN method for FSE. Another important outcome of this work is the demonstration of the suitability of the discussed model for both LV and MV grids.

The primary aim of our future work is to combine TSE and HSE based on the presented HSE model. Next, the TSE will be implemented by adapting the ANN's input to a dynamic structure that handles various spectral datasets. As a Gaussian layer already improved the prediction of states based on noisy measurements, the PM will be tested in laboratory grids, too. Finally, another future task is the implementation of a controlling module, which ensures the accordance of estimated states to physical laws.

Author Contributions: Conceptualization, P.M. and M.d.K.; methodology, P.M., M.d.K. and P.L.; software, P.M. and M.d.K.; validation, M.d.K. and P.M.; formal analysis, M.d.K. and P.M.; resources, M.d.K. and P.M.; data curation, M.d.K.; writing—original draft preparation, P.M.; writing—review and editing, P.M., M.d.K. and P.L.; visualization, P.M. and M.d.K.; supervision, E.W. and I.S.; project administration, E.W., P.M. and P.L.; funding acquisition, E.W. and I.S. All authors have read and agreed to the published version of the manuscript.

Funding: This research was funded by the German Federal Ministry for Economic Affairs and Climate Action grant number 03EI4048R.

Data Availability Statement: Used code and data are available on GitHub (https://github.com/th-koeln-iet/pqse_concept_pann (accessed on 27 October 2024)) and Zenodo (https://zenodo.org/records/13122171 (accessed on 27 October 2024)). Detailed instructions to reproduce results may be found on GitHub.

Conflicts of Interest: The authors declare no conflicts of interest. The funders had no role in the design of the study; in the collection, analyses, or interpretation of data; in the writing of the manuscript; or in the decision to publish the results.

Appendix A

Table A1. Harmonic spectra used in validation and test data sets [52,53].

Grid	Node	Type	Ord.	1	2	3	4	5	6	7	8	9	10	11	12	13	14	15	16	17	18	19	20
													Magnitude [%]										
CIGRE LV	9, 32, 35	PV		99.96	0.326	0.451	0.218	1.797	0.039	2.23	0.24	0.13	0.164	0.236	0.011	0.083	0.042	0.016	0.034	0.018	0.002	0.022	0.011
CIGRE LV	16, 17, 37, 41, 42	EVSE		100	-	8.4	-	2.1	-	3.6	-	1.3	-	1.2	-	0.4	-	0.3	-	0.3	-	0.01	-
IEEE33-bus	13, 17, 20, 23, 28	EVSE		100	-	8.4	-	2.1	-	3.6	-	1.3	-	1.2	-	0.4	-	0.3	-	0.3	-	0.01	-
													Phase [°]										
CIGRE LV	9, 32, 35	PV		76.96	−94.8	33.034	146.2	−178.5	118.52	101.36	−101.2	−17.26	86.05	72.84	−124.3	53.56	−113.0	5.499	78.59	−98.51	−157.2	165.56	−80.66
CIGRE LV	16, 17, 37, 41, 42	EVSE		0.0	-	0.0	-	0.0	-	0.0	-	0.0	-	0.0	-	0.0	-	0.0	-	0.0	-	0.0	-
IEEE33-bus	13, 17, 20, 23, 28	EVSE		0.0	-	0.0	-	0.0	-	0.0	-	0.0	-	0.0	-	0.0	-	0.0	-	0.0	-	0.0	-

Table A2. Power systems' loads and generators.

IEEE33-bus				CIGRE LV			
Names	Node	P [kW]	Q [kvar]	Names	Node	P [kW]	Q [kvar]
1	1	0–100	0–60	R1	2	0–190	0–62.45
2, 17, 18, 19, 20, 21	2, 17, 18, 19, 20, 21	0–90	0–40	R11	12	0–14.25	0–4.684
3, 13	3, 13	0–120	0–80	R15	16	0–49.4	0–16.237
4	4	0–60	0–30	R16	17	0–52.25	0–17.174
5, 8, 9, 15, 16, 27	5, 8, 9, 15, 16, 27	0–60	0–20	R17	18	0–33.25	0–10.929
6, 7	6, 7	0–200	0–100	R18	19	0–44.65	0–14.676
10	10	0–45	0–30	I2	22	0–85	0–52.307
11, 12	11, 12	0–60	0–35	C1	24	0–108	0–52.307
14	14	0–60	0–10	C12, C13	35, 36	0–18	0–8.718
22	22	0–90	0–50	C14, C17	37, 40	0–22.5	0–10.897
23, 24	23, 24	0–420	0–200	C18, C20	41, 43	0–7.2	0–3.487
25, 26	25, 26	0–60	0–25	C19	42	0–7.2	0–3.487
28	28	0–120	0–70	PV1	9	0–10	0
29	29	0–200	0–600	PV2	32	0–35	0
30	30	0–150	0–70	PV3	35	0–15	0
31	31	0–210	0–100				
32	32	0–60	0–40				

References

1. Schulz, D. *Mains Disturbances—Theory, Simulation, Measurement and Evaluation: Per DIN VDE 0838, DIN VDE 0839 and the VDEW-Guidelines with Simulation-Examples in Simplorer and Measurements of Grid-Connected Photovoltaic Systems and Wind Power Generators, VDE-Schriftenreihe Normen Verständlich*, 1st ed.; VDE-Verl.: Berlin/Offenbach, Germany, 2004; Volume 115, p. 14. (In German)
2. *DIN EN 50160:2020-11*; Voltage Characteristics of Electricity Supplied by Public Electricity Networks. DIN Media GmbH: Berlin, Germany, 2020.
3. *EN61000-2-2:2020-05*; Electromagnetic Compatibility (EMC)—Part 2-2: Environment—Compatibility Levels for Low-Frequency Conducted Disturbances and Signalling in Public Low-Voltage Power Supply Systems. DIN Media GmbH: Berlin, Germany, 2020.
4. Phadke, A.G.; Bi, T. Phasor measurement units, WAMS, and their applications in protection and control of power systems. *J. Mod. Power Syst. Clean Energy* **2018**, *6*, 619–629. [CrossRef]
5. Watson, N.R. Power quality state estimation. *Eur. Trans. Electr. Power* **2010**, *20*, 19–33. [CrossRef]
6. Sanchez-Puentes, Y.; Argote-Parra, C.; Lakatt-Benavides, W.; Narvaez-Viana, J.; Nuñez-Alvarez, J.; Grimaldo-Guerrero, J. Influence of Photovoltaic Systems on Power Quality Problems. *Int. J. Energy Econ. Policy* **2023**, *13*, 185–190. [CrossRef]
7. Ping, H.; Dong, L.; Xin, Q. Influence of Grid-connected Photovoltaic Systems on Power Quality. In Proceedings of the 2019 IEEE 2nd International Conference on Automation, Electronics and Electrical Engineering (AUTEEE), Shenyang, China, 22–24 November 2019.
8. Gomez, J.C.; Morcos, M.M. Impact of EV battery chargers on the power quality of distribution systems. *IEEE Trans. Power Deliv.* **2003**, *18*, 975–981. [CrossRef]
9. Bohn, J.K.; McMullen, D.W.; Save, P. *Electric Vehicle Battery Charger Harmonics Study*; EPRI: Palo Alto, CA, USA, 1995.
10. Alliance for Telecommunications Industry Solutions. Federal Standard 1037C: Glossary of Telecommunications Terms. Available online: https://glossary.atis.org (accessed on 13 May 2024).
11. *519-2022*; IEEE Standard for Harmonic Control in Electric Power Systems. IEEE: Piscataway, NJ, USA, 2022.
12. Melo, I.D.; Pereira, J.L.; Variz, A.M.; Garcia, P.A. Harmonic state estimation for distribution networks using phasor measurement units. *Electr. Power Syst. Res.* **2017**, *147*, 133–144. [CrossRef]
13. Breda, J.F.; Vieira, J.C.M.; Oleskovicz, M. Three-phase harmonic state estimation for distribution systems by using the SVD technique. In Proceedings of the 2016 IEEE Power and Energy Society General Meeting (PESGM), Boston, MA, USA, 17–21 July 2016; pp. 1–5.
14. Bhujel, D.; Watson, N.R.; Jalal, T.S. Application of harmonic state estimation to a distribution system. In Proceedings of the 2017 IEEE Manchester PowerTech, Manchester, UK, 18–22 June 2017; pp. 1–6.
15. Zang, T.; Wang, Y.; Sun, H.; He, Z. Variable parameter Kalman filter based dynamic harmonic state estimation for power systems with wind energy integration. In Proceedings of the 2017 IEEE Conference on Energy Internet and Energy System Integration (EI2), Beijing, China, 26–28 November 2017; pp. 1–5.
16. Shaghaghi, A.; Zahedi, R.; Ghorbani, M.; Ranjbar, Z.; Arzhangi, S.S.; Keshavarzzadeh, M.; Alipour, H. State estimation for distribution power systems by applying an advanced optimization approach. *Expert Syst. Appl.* **2024**, *240*, 122325. [CrossRef]
17. Schweppe, F.; Wildes, J. Power System Static-State Estimation, Part I: Exact Model. *IEEE Trans. Power Appar. Syst.* **1970**, *PAS-89*, 120–125. [CrossRef]
18. Lin, G. *State Estimation in Medium Voltage Grids with Incomplete Measurement Infrastructure*; Cuvillier Verlag: Göttingen, Germany, 2019; pp. 44, 57. (In German)
19. Kelker, M.; Schulte, K.; Kroger, K.; Haubrock, J. Development and validation of a neural network for state estimation in the distribution grid based on uPMU data. In Proceedings of the 2019 Modern Electric Power Systems (MEPS), Wroclaw, Poland, 9–12 September 2019; pp. 1–6.
20. Manitsas, E.; Singh, R.; Pal, B.C.; Strbac, G. Distribution System State Estimation Using an Artificial Neural Network Approach for Pseudo Measurement Modeling. *IEEE Trans. Power Syst.* **2012**, *27*, 1888–1896. [CrossRef]
21. Bahabadi, H.B.; Mirzaei, A.; Moallem, M. Optimal Placement of Phasor Measurement Units for Harmonic State Estimation in Unbalanced Distribution System Using Genetic Algorithms. In Proceedings of the 2011 21st International Conference on Systems Engineering, Las Vegas, NA, USA, 16–18 August 2011; pp. 100–105.
22. Arefi, A.; Haghifam, M.R.; Fathi, S.H. Distribution harmonic state estimation based on a modified PSO considering parameters uncertainty. In Proceedings of the 2011 IEEE Trondheim PowerTech, Trondheim, Norway, 9–23 June 2011; pp. 1–7.
23. Arefi, A.; Haghifam, M.R.; Fathi, S.H.; Niknam, T.; Olamaei, J. A novel algorithm based on Honey Bee Mating Optimization for distribution harmonic state estimation including distributed generators. In Proceedings of the 2009 IEEE Bucharest PowerTech, Bucharest, Romania, 28 June–2 July 2009; pp. 1–7.
24. Zhou, W.; Ardakanian, O.; Zhang, H.T.; Yuan, Y. Bayesian Learning-Based Harmonic State Estimation in Distribution Systems With Smart Meter and DPMU Data. *IEEE Trans. Smart Grid* **2020**, *11*, 832–845. [CrossRef]
25. Xie, Y.; Shao, Z.; Chen, F.; Lin, H. Harmonic State Estimation Based on Network Equivalence and Closed Loop GAN. In Proceedings of the 2023 8th Asia Conference on Power and Electrical Engineering (ACPEE), Tianjin, China, 14–16 April 2023; pp. 1688–1693.

26. Tran, M.Q.; Zamzam, A.S.; Nguyen, P.H.; Pemen, G. Multi-Area Distribution System State Estimation Using Decentralized Physics-Aware Neural Networks. *Energies* **2021**, *14*, 3025. [CrossRef]
27. Zamzam, A.S.; Sidiropoulos, N.D. Physics-Aware Neural Networks for Distribution System State Estimation. *IEEE Trans. Power Syst.* **2020**, *35*, 4347–4356. [CrossRef]
28. Farzanehrafat, A.; Watson, N.R. Power Quality State Estimator for Smart Distribution Grids. *IEEE Trans. Power Syst.* **2013**, *28*, 2183–2191. [CrossRef]
29. Marini, A.; Shabanzadeh, M.; Esmaeili, A. Chapter 8.2—Power quality state estimation of power distribution systems: Opportunities and challenges in observability enhancement. In *Active Electrical Distribution Network: Issues, Solution Techniques, and Applications*; Padmanaban, S., Khan, B., Mahela, O.P., Alhelou, H.H., Rajkumar, S., Eds.; Academic Press: Cambridge, MA, USA, 2022; pp. 243–284.
30. Cooley, J.W.; Tukey, J.W. An algorithm for the machine calculation of complex Fourier series. *Math. Comput.* **1965**, *90*, 297–301. [CrossRef]
31. Ametani, A. The Application of the Fast Fourier Transform to Electrical Transient Phenomena. *Int. J. Electr. Eng. Educ.* **1973**, *10*, 277–287. [CrossRef]
32. Tavighi, A.; Ahmadi, H.; Armstrong, M.; Martí, J.R. Discrete-Time Fourier Series to simulate transient over voltages in power systems. *Electr. Power Syst. Res.* **2020**, *188*, 106529. [CrossRef]
33. Li, B.; Jiang, Z.; Chen, J. On Performance of Sparse Fast Fourier Transform Algorithms Using the Flat Window Filter. *IEEE Access* **2020**, *8*, 79134–79146. [CrossRef]
34. Aggarwal, C.C. *Neural Networks and Deep Learning: A Textbook*, 2nd ed.; Springer International Publishing and Imprint Springer: Cham, Switzerland, 2023; pp. 1164130–1164131.
35. Haykin, S.S. *Neural Networks and Learning Machines*, 3rd ed.; Pearson: New York, NY, USA, 2009; pp. 10–24.
36. Fukushima, K. Visual Feature Extraction by a Multilayered Network of Analog Threshold Elements. *IEEE Trans. Syst. Sci. Cybern.* **1969**, *5*, 322–333. [CrossRef]
37. Mahseredjian, J.; Dinavahi, V.; Martinez, J.A. Simulation Tools for Electromagnetic Transients in Power Systems: Overview and Challenges. *IEEE Trans. Power Deliv.* **2009**, *24*, 1657–1669. [CrossRef]
38. CIGRE. *Benchmark Systems for Network Integration of Renewable and Distributed Energy Resources: Task Force C6.04; Brochures Thématiques*; CIGRE: Paris, France, 2014; Volume 575.
39. Baran, M.E.; Wu, F.F. Network reconfiguration in distribution systems for loss reduction and load balancing. *IEEE Trans. Power Deliv.* **1989**, *4*, 1401–1407. [CrossRef]
40. Dugan, R.C.; Montenegro, D.; Ballanti, A. *Reference Guide the Open Distribution Simulator (OpenDSS 9.0.0)*; EPRI: Palo Alto, CA, USA, 2020.
41. Scheidler, A.; Thurner, L. pandapower v2.13.1. Available online: https://pandapower.readthedocs.io/en/v2.13.1/std_types/basic.html#lines (accessed on 12 June 2024).
42. Oeding, D.; Oswald, B.R. *Electrical Power Plants and Grids*; Springer: Berlin/Heidelberg, Germany, 2016; p. 229. (In German)
43. de Koster, M.; Mack, P.; Lehnen, P. Code and Data Repository QUIRINUS Control. Available online: https://github.com/th-koeln-iet/pqse_concept_pann (accessed on 30 July 2024).
44. Kingma, D.P.; Ba, J. Adam: A Method for Stochastic Optimization. *arXiv* **2014**, arXiv:1412.6980.
45. Sammut, C.; Webb, G.I. (Eds.) *Encyclopedia of Machine Learning and Data Mining*, 2nd ed.; Springer Reference; Springer: New York, NY, USA, 2017; p. 808.
46. Willmott, C.J.; Matsuura, K. Advantages of the mean absolute error (MAE) over the root mean square error (RMSE) in assessing average model performance. *Clim. Res.* **2005**, *30*, 79–82. [CrossRef]
47. Janssen, P.; Heuberger, P. Calibration of process-oriented models. *Ecol. Model.* **1995**, *83*, 55–66. [CrossRef]
48. Ahmadi-Gorjayi, F.; Mohsenian-Rad, H. A Physics-Aware MIQP Approach to Harmonic State Estimation in Low-Observable Power Distribution Systems Using Harmonic Phasor Measurement Units. *IEEE Trans. Smart Grid* **2023**, *14*, 2111–2124. [CrossRef]
49. Wang, Y.; Ma, H.; Xiao, X.; Wang, Y.; Zhang, Y.; Wang, H. Harmonic State Estimation for Distribution Networks Based on Multi-Measurement Data. *IEEE Trans. Power Deliv.* **2023**, *38*, 2311–2325. [CrossRef]
50. Brown, M.; Biswal, M.; Brahma, S.; Ranade, S.J.; Cao, H. Characterizing and quantifying noise in PMU data. In Proceedings of the 2016 IEEE Power and Energy Society General Meeting (PESGM), Boston, MA, USA, 17–21 July 2016; pp. 1–5.
51. Zhang, L.; Wang, G.; Giannakis, G.B. Real-Time Power System State Estimation and Forecasting via Deep Unrolled Neural Networks. *IEEE Trans. Signal Process.* **2019**, *67*, 4069–4077. [CrossRef]
52. Arritt, R.; Dugan, R. *Validation of Harmonic Models for PV Inverters: PV-MOD Milestone 2.8.2*; Electric Power Research Institute (EPRI): Washington, DC, USA, 2022.
53. Idaho National Laboratory. Steady State Vehicle Charging Fact Sheet: 2014 BMW i3. Available online: https://avt.inl.gov/sites/default/files/pdf/fsev/SteadyStateLoadCharacterization2014BMWi3.pdf (accessed on 16 October 2024).

Disclaimer/Publisher's Note: The statements, opinions and data contained in all publications are solely those of the individual author(s) and contributor(s) and not of MDPI and/or the editor(s). MDPI and/or the editor(s) disclaim responsibility for any injury to people or property resulting from any ideas, methods, instructions or products referred to in the content.